

# 光学学报

## 空间引力波望远镜远场相位噪声抑制方法

陈胜楠<sup>\*\*</sup>, 王春艳<sup>\*\*\*</sup>, 孙浩, 姜会林<sup>\*</sup>

长春理工大学光电工程学院, 吉林 长春 130033

**摘要** 空间引力波望远镜的波像差与指向抖动耦合产生的远场相位噪声是引力波探测的主要噪声源。基于其产生的理论机制,建立了噪声耦合系数与望远镜像差间的函数关系,提出了控制特定像差的优化策略。结合望远镜设计实例验证了该方法对抑制远场相位噪声的效果,当波前质量水平为  $\lambda/20$  ( $\lambda=1064$  nm) 时,优化后的噪声耦合系数优于  $0.11$  pm/nrad,较优化前降低了一个数量级,远优于指标要求,所提方法极大地提升了望远镜的远场相位稳定性。

**关键词** 激光光学; 望远镜; 空间引力波探测; 远场相位; 耦合系数

中图分类号 O439 文献标志码 A

DOI: 10.3788/AOS222100

空间引力波探测中,激光信号(1064 nm)通过望远镜进行收发<sup>[1-2]</sup>。望远镜采用离轴四反无焦光学系统,后端承接成像系统,激光束腰位于全系统出瞳处<sup>[3-4]</sup>。由望远镜抖动(10 nrad/Hz<sup>1/2</sup>量级)和像差相互作用引起的相位噪声影响着系统的测量精度。该相位噪声包括两种:出射端抖动产生的远场相位噪声和接收端抖动产生的外差信号相位噪声。望远镜设计的主要要求之一是提升系统的光程稳定性,以降低指向抖动对相位的影响,通常要求两种相位噪声总的耦合系数小于苛刻的 1 pm/nrad<sup>[5]</sup>。2019年,Sasso等<sup>[5-7]</sup>研究了不同波前质量下的噪声耦合系数。2020年,Zhao等<sup>[8]</sup>进一步研究了外差信号相位噪声的抑制方法。这些研究均以整体波前质量(均方根RMS值等)作为评价参数,并通过基于像差随机采样的蒙特卡罗仿真得出对波前质量的要求。但仿真结果也表明相同的波前质量下的相位噪声差异悬殊<sup>[5-8]</sup>,这说明不同像差对噪声的贡献不同,简单地以整体波前质量作为评价参数不够精确,导致对波前质量的要求过于严格。实际上,望远镜的像差并非随机分布,而是可以被针对性控制的。2022年,本课题组<sup>[9]</sup>针对外差相位噪声,提出了控制特定像差的噪声抑制方法,首次通过光学设计突破性地减小了噪声耦合系数。本文首次针对远场相位噪声,建立像差成分与耦合系数的关系,通过对关键像差的优化设计将耦合系数减小了一个数量级,极大地降低了远场相位稳定性对望远镜波前质量的要求。

图 1 为出射端望远镜系统原理图,拟定口径为 400 mm(半径  $r_0=200$  mm),放大倍率为 200(望远镜的放大倍率为 80,Kepler 成像系统的放大倍率为

2.5),科学视场为  $\pm 8$   $\mu$ rad,测量臂长为  $2.5 \times 10^9$  m。

激光高斯光束经准直出射后,接收端望远镜(口径为  $S$ )轴上距离  $z$  处的远场振幅<sup>[6]</sup>为

$$u(0, z) = \frac{ik}{2\pi z} \int_S \exp(-r^2/w^2) e^{i2\pi W_0(\rho, \theta)} ds, \quad (1)$$

式中:  $W_0(\rho, \theta)$  表示出射光束的归一化( $\rho=r/r_0$ )波前误差;  $(\rho, \theta)$  表示口径极坐标。远场波前误差  $W_E$  可通过远场波前相位  $\phi_{\text{far}}$ (振幅求辐角)计算得到<sup>[5-6]</sup>:

$$W_E = \frac{\lambda}{2\pi} \phi_{\text{far}}(0, z) = \frac{\lambda}{2\pi} \arg[u(0, z)]. \quad (2)$$

设计阶段,忽略高阶像差,利用条纹泽尼克多项式  $Z_i(\rho, \theta)$  的前 15 项(忽略 piston 即第一项)拟合  $W_0(\rho, \theta)$ :

$$W_0(\rho, \theta) = \sum_{i=2}^{15} C_i Z_i(\rho, \theta), \quad (3)$$

式中:  $C_i$  为多项式系数。在子午和弧矢面内的波前倾斜( $\alpha, \beta$ )可表示为

$$\begin{cases} \alpha = \frac{C_3 \lambda}{r_0} \\ \beta = \frac{C_2 \lambda}{r_0} \end{cases} \quad (4)$$

波前误差的 RMS 值  $\sigma_w$ (不考虑倾斜)<sup>[10]</sup>为

$$\begin{cases} N_i^{nm} = \sqrt{\frac{2(n+1)}{1+\delta_{m0}}} \\ \sigma_w = \sqrt{\sum_{i=2}^{15} \left( \frac{C_i}{N_i^{nm}} \right)^2} \end{cases}, \quad (5)$$

式中:  $\delta_{m0}$  为克罗内克  $\delta$  函数。将  $\exp[i2\pi W_0(\rho, \theta)]$  在  $i2\pi W_0(\rho, \theta)=0$  的三阶泰勒展开与式(3)、(4)代入式(1)、(2),则

收稿日期: 2022-12-05; 修回日期: 2023-01-17; 录用日期: 2023-02-08; 网络首发日期: 2023-02-18

基金项目: 吉林省教育厅资助(JJKH20220755KJ)

通信作者: \*hljiang@cust.edu.cn; \*\*865666068@qq.com; \*\*\*245044961@qq.com

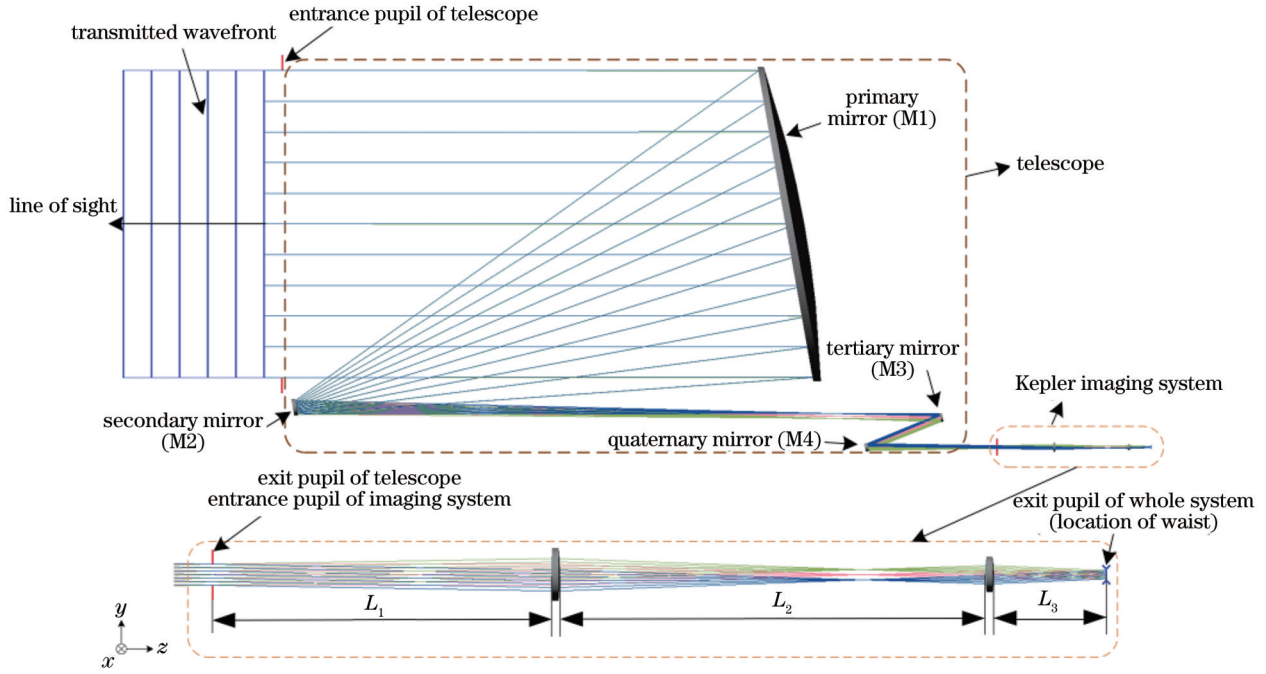


图 1 望远镜系统原理图

Fig. 1 Schematic diagram of telescope system

$$W_E(\alpha, \beta) \approx b_{00} + b_{10}\beta + b_{20}\beta^2 + b_{01}\alpha + b_{02}\alpha^2 + b_{11}\alpha\beta, \quad (6)$$

式中:系数  $b_{ij}$  是像差系数  $C_i$  的多项式函数  $f_{ij}(C_4, C_5, \dots, C_{15})$ 。 $W_E$  的单位为 pm,  $\alpha$  和  $\beta$  的单位为 nrad。可见,视轴抖动,即  $\alpha$  和  $\beta$  的微弱变化将导致远场波前发生变化。考虑最差的情况,定义噪声耦合系数  $\delta_{far}(\alpha, \beta)$  为远场波前误差  $W_E(\alpha, \beta)$  的梯度的模 ( $|\text{grad } W_E(\alpha, \beta)|$ ), 则有

$$\delta_{far}^2(\alpha, \beta) = (b_{10} + 2b_{20}\beta + b_{11}\alpha)^2 + (b_{01} + 2b_{02}\alpha + b_{11}\beta)^2. \quad (7)$$

式(7)中  $\delta_{far}$  的单位为 pm/nrad,  $b_{10}$  和  $b_{01}$  各包含 188 项,  $b_{20}$  和  $b_{02}$  各包含 27 项,  $b_{11}$  包含 17 项。可见,抑制  $\delta_{far}(\alpha, \beta)$  是一个针对像差系数的极其复杂的多变量优化问题,简单地通过控制整体波前质量难以直接有效地抑制相位噪声,需要进一步分析并简化像差与耦合系数的关系。

重点分析中心视场(子午面内),考虑望远镜的对称性,包含  $\cos \theta$  的像差的系数  $C_i$  (即  $C_6, C_7, C_{10}, C_{13}$  和  $C_{14}$ ) 均为 0。取束腰  $w$  为 200 mm, 得到

$$\begin{cases} b_{10} = 0 \\ b_{01} = (-500.781C_4 + 64.2690C_5 - 277.952C_9 + 252.503C_{12})C_8 + 112.086C_4C_{15} - 355.766C_5C_{11} - \\ \quad 21.7829C_5C_{15} - 319.713C_9C_{15} - 29.8482C_{11}C_{12} + 75.0006C_{12}C_{15} \\ b_{20} = -0.0588662C_4 - 0.0471348C_5 + 0.0118003C_9 + 0.00765783C_{12} \\ b_{02} = -0.0588662C_4 + 0.0471348C_5 + 0.0118003C_9 - 0.00765783C_{12} \\ b_{11} = 0 \end{cases}, \quad (8)$$

$$\delta_{far}(\alpha, \beta) = \sqrt{(2b_{20}\beta)^2 + (b_{01} + 2b_{02}\alpha)^2}. \quad (9)$$

忽略  $W_0(r, \theta)$  对能量的影响,图 2 为接收端光强度的归一化分布  $|u_{0z}(\alpha, \beta)|^2 / |u_{0z}(0, 0)|^2$  [ $u_{0z}(\alpha, \beta)$  为接收端望远镜轴上振幅随倾斜程度变化的函数]。可见,波前倾斜越大,能量下降越明显。为确保足够高的能量传播效率,下文重点分析中心视场附近直径为 200 nrad 的圆域(直径为 500 m)。在轨运行时,平台会适时修正望远镜的指向,确保望远镜持续指向目标视场附近<sup>[11]</sup>。

直接将式(9)作为优化目标的一部分,会导致优化函数过于复杂,难以收敛。望远镜的像差系数  $C_i$  可通过优化结构参数进行控制。为提高计算效率,根据像差特性提炼优化策略。在离轴四反无焦系统的残差中,初级彗差( $C_8$ )相对较大,难以减小,而三叶草像差、二阶像散和二阶彗差( $C_{11}, C_{12}$  和  $C_{15}$ )相对较小,且在优化时相对稳定。根据式(9),  $|b_{01}|$  决定了中心视场  $\delta_{far}(\alpha, \beta)$  的大小,  $b_{20}$  和  $b_{02}$  则决定了  $\delta_{far}(\alpha, \beta)$  随角度的变化速率。因此,在优化过程中需抑制  $C_8$  的系数表达式  $(-500.781C_4 + 64.2690C_5 - 277.952C_9)$  以重点减小

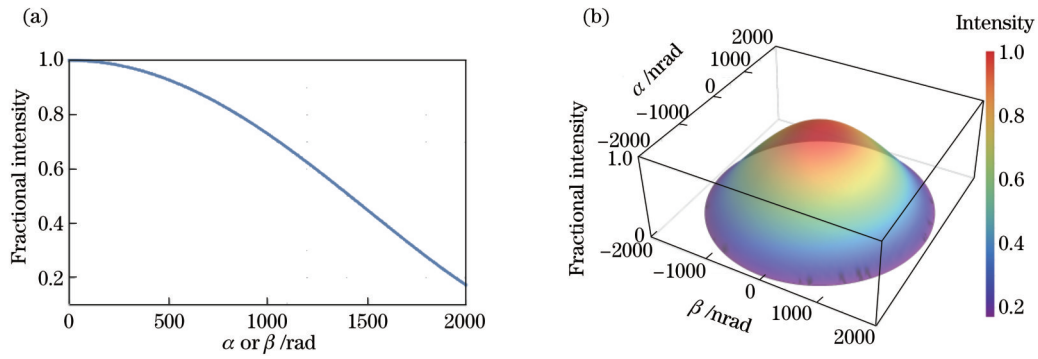


图 2 接收能量归一化分布。(a)强度分布曲线;(b)强度分布图

Fig. 2 Normalized distributions of received energy. (a) Intensity distribution curve; (b) intensity distribution

$b_{01}$ , 并依序减小  $C_4$ 、 $C_5$  和  $C_9$  以均衡地控制  $b_{01}$ 、 $b_{20}$  和  $b_{02}$ 。

下面通过实例验证上述策略对耦合系数的抑制效果。首先,在一定的约束条件下,基于整体波前误差的优化函数对望远镜进行优化设计,得到 System1。然后按照上述策略进行进一步优化,得到 System2。此过程中只优化望远镜的结构参数,而 Kepler 成像系统

的结构参数<sup>[9]</sup>保持不变。两系统的结构参数(包括曲率半径  $R$ 、二次曲面系数  $k$ 、反射镜相对主镜的位置和倾斜角度)见表 1。优化前后,全系统波前误差的  $C_i$  和  $\sigma_w$  见表 2,  $|b_{01}|$ 、 $|b_{20}|$  和  $|b_{02}|$  分别从  $3.48 \times 10^{-1}$ 、 $2.83 \times 10^{-3}$  和  $5.98 \times 10^{-3}$  减小至  $1.34 \times 10^{-2}$ 、 $3.23 \times 10^{-4}$  和  $3.29 \times 10^{-4}$ 。

表 1 System1 和 System2 中望远镜的结构参数

Table 1 Structural parameters of telescopes in System1 and System2

Telescope	Mirror	$R / \text{mm}$	$k$	$y / \text{mm}$	$z / \text{mm}$	Tilt / ( $^\circ$ )
Telescope in System1	M1	—	—	0	0	0
	M2	-66.21	—	0	673.65	—
	M3	-564.69	—	0	165.11	10.773
	M4	746.09	—	—	79.75	14.137
				80.36		
Telescope in System2	M1	—	—	0	0	0
	M2	-66.15	—	0	—	0
	M3	-577.70	—	0	193.16	10.809
	M4	816.85	—	—	116.88	14.011
				78.95		

表 2 System1 和 System2 的  $C_i$  及其  $\sigma_w$ Table 2  $C_i$  and corresponding  $\sigma_w$  of System1 and System2

Term	System1	System2
$C_4$	$-2.55463 \times 10^{-2} \lambda$	$-3.61899 \times 10^{-5} \lambda$
$C_5$	$-9.37489 \times 10^{-2} \lambda$	$6.59153 \times 10^{-3} \lambda$
$C_8$	$-7.98534 \times 10^{-2} \lambda$	$-1.45964 \times 10^{-1} \lambda$
$C_9$	$6.15331 \times 10^{-3} \lambda$	$-4.14483 \times 10^{-4} \lambda$
$C_{11}$	$8.99012 \times 10^{-4} \lambda$	$2.91833 \times 10^{-3} \lambda$
$C_{12}$	$-1.36633 \times 10^{-3} \lambda$	$-2.02830 \times 10^{-3} \lambda$
$C_{15}$	$7.37880 \times 10^{-4} \lambda$	$1.33327 \times 10^{-3} \lambda$
$\sigma_w$	0.0499 $\lambda$	0.0517 $\lambda$

图 3 以 System1 为例,对比了解析计算[式(6)和(8)]和数值计算[式(2)] $W_E(\alpha, \beta)$ 的结果,子午面和弧矢面内的平均误差小于 2 pm,可见解析计算的精度较高。由式(6)计算 System1 和 System2 的  $W_E(\alpha, \beta)$ ,见图 4。可见,优化后,  $W_E(\alpha, \beta)$  的变化范围明显减小(降幅超过 90%)。图 5 为 System1 和 System2 的  $\delta_{far}(\alpha, \beta)$ ,可见 System1 的  $\delta_{far}$  随角度的增加而大于 1 pm/nrad。相较于 System1,尽管 System2 的  $\sigma_w$  略有增加,但优化后,在 200 nrad 范围内,其  $\delta_{far}$  被降至可被忽略的水平(最大值为 0.11 pm/nrad,约为 System1 的 6.0%)。上述论述针对中心视场,经分析,科学视场内 System2 的  $\delta_{far}$  均相应减小,足见针对性控制像差的优

化策略对于抑制远场相位噪声的效果显著。从图 5 也可看出,寻找最优倾斜的方法也可在一定程度上减小  $\delta_{far}$ ,但与该优化方法相比,收效甚微<sup>[6]</sup>。

更为重要的是, System2 的波前质量不及  $\lambda/20$ ,是现有研究限定的公差要求的 3 倍以上。可见该方法在波前质量较差的情况下依然可以有效地抑制远场相位噪声,突破了通过严控波前质量来降低噪声的固有思路,有效缓解了苛刻的噪声预算与系统可实现性间的矛盾,同时为望远镜的加工和装调提供了理论指导。综合考虑远场和外差信号相位噪声的抑制对望远镜波前像差的要求,研究抑制由抖动产生的总相位噪声的优化方法是本课题组下一步工作的重要内容。

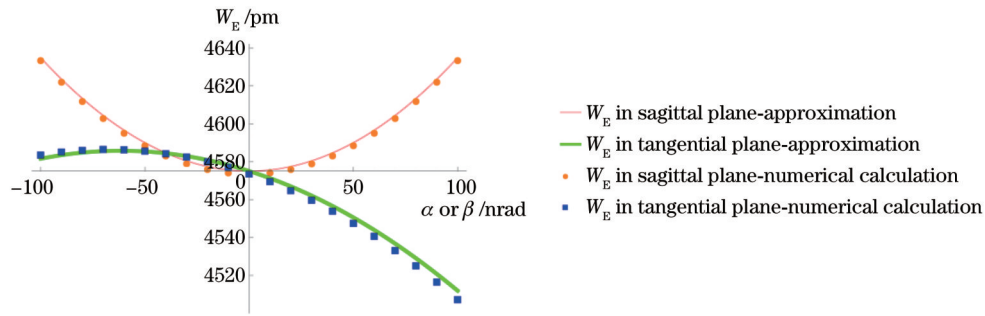


图 3  $W_E(\alpha, \beta)$  的解析与数值计算对比

Fig. 3 Comparison of analytical and numerical calculations of  $W_E(\alpha, \beta)$

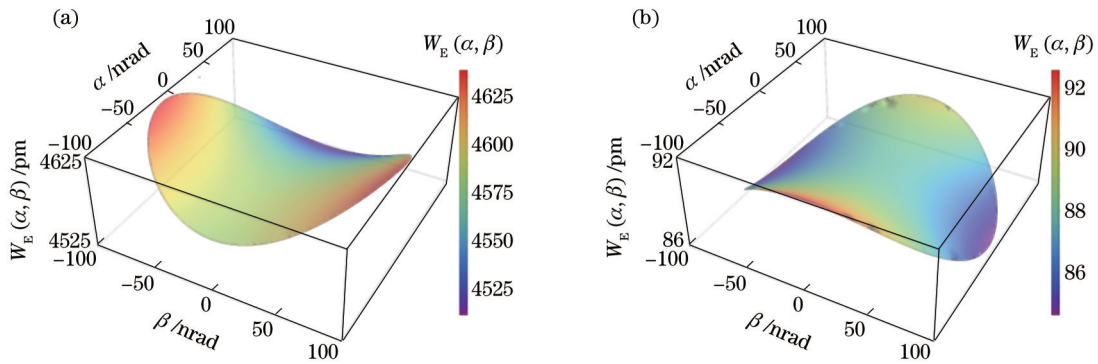


图 4 System1 和 System2 的  $W_E(\alpha, \beta)$ 。(a) System1; (b) System2

Fig. 4  $W_E(\alpha, \beta)$  of System1 and System2. (a) System1; (b) System2

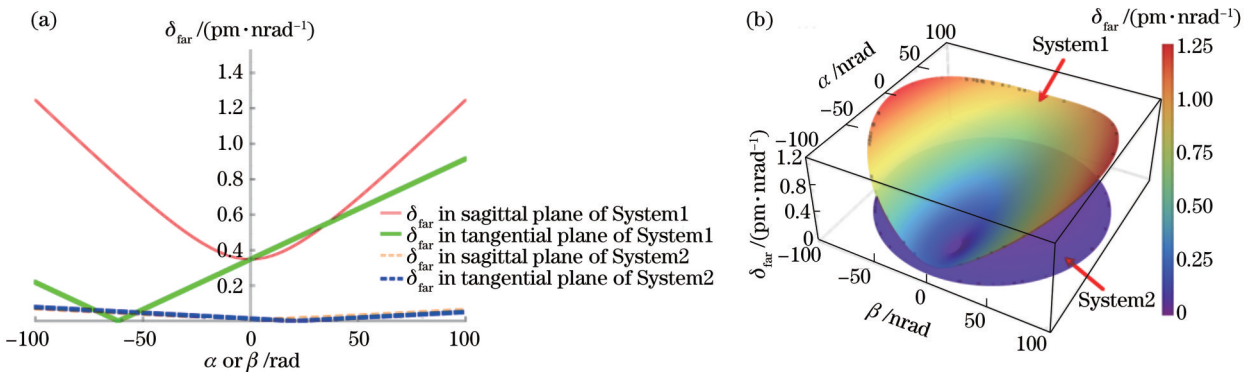


图 5 System1 和 System2 的  $\delta_{far}(\alpha, \beta)$ 。(a) 子午面和弧矢面内的  $\delta_{far}(\alpha, \beta)$ ; (b) System1 和 System2 的  $\delta_{far}(\alpha, \beta)$

Fig. 5  $\delta_{far}(\alpha, \beta)$  of System1 and System2. (a)  $\delta_{far}(\alpha, \beta)$  in sagittal and tangential planes; (b)  $\delta_{far}(\alpha, \beta)$  of System1 and System2

## 参 考 文 献

- [1] Schuster S. Tilt-to-length coupling and diffraction aspects in satellite interferometry[D]. Hannover: Gottfried Wilhelm Leibniz Universitaet Hannover, 2017.
- [2] Hu W R, Wu Y L. The Taiji Program in Space for gravitational wave physics and the nature of gravity[J]. National Science Review, 2017, 4(5): 685-686.
- [3] Schuster S, Tröbs M, Wanner G, et al. Experimental demonstration of reduced tilt-to-length coupling by a two-lens imaging system[J]. Optics Express, 2016, 24(10): 10466-10475.
- [4] Livas J C, Arsenovic P, Crow J A, et al. Telescopes for space-based gravitational wave missions[J]. Optical Engineering, 2013, 52(9): 091811.
- [5] Sasso C P, Mana G, Mottini S. Telescope jitters and phase noise in the LISA interferometer[J]. Optics Express, 2019, 27(12): 16855-16870.
- [6] Sasso C P, Mana G, Mottini S. Coupling of wavefront errors and jitter in the LISA interferometer: far-field propagation[J]. Classical and Quantum Gravity, 2018, 35(18): 185013.
- [7] Sasso C P, Mana G, Mottini S. Coupling of wavefront errors and pointing jitter in the LISA interferometer: misalignment of the interfering wavefronts[J]. Classical and Quantum Gravity, 2018, 35(24): 245002.
- [8] Zhao Y, Shen J, Fang C, et al. Tilt-to-length noise coupled by wavefront errors in the interfering beams for the space measurement of gravitational waves[J]. Optics Express, 2020, 28(17): 25545-25561.
- [9] Chen S N, Wang C Y, Jiang H L, et al. Reducing phase noise coupled by wavefront errors in optical telescopes for the space measurement of gravitational waves[J]. Optics Express, 2022, 30(21): 37648-37663.
- [10] Lakshminarayanan V, Fleck A. Zernike polynomials: a guide[J]. Journal of Modern Optics, 2011, 58(7): 545-561.
- [11] Dong Y H, Liu H S, Luo Z R, et al. Methodological demonstration of laser beam pointing control for space gravitational wave detection missions[J]. The Review of Scientific Instruments, 2014, 85(7): 074501.

## Method of Far-Field Phase Noise Suppression for Space Gravitational-Wave Detection Telescope

Chen Shengnan<sup>\*\*</sup>, Wang Chunyan<sup>\*\*\*</sup>, Sun Hao, Jiang Huilin<sup>\*</sup>

*School of Opto-Electronic Engineering, Changchun University of Science and Technology, Changchun 130033, Jilin, China*

### Abstract

**Objective** Space-based gravitational-wave observatories (SGOs) promise to measure pico-meter variations in the gigameter separations of a triangular constellation. Telescopes play a crucial role in using transmitting and receiving laser beams measuring the constellation arms with heterodyne laser interferometry. The far-field phase noise induced by the coupling of the wavefront aberrations of optical telescopes with their pointing jitters is one of the major noise sources for the measurement. As phase noise suppression is a critical aspect for achieving the required comprehensive measuring stability, this paper theoretically analyzes the mechanism of the far-field phase noise, proposes an optimization strategy for the design of the optical telescopes in SGOs, and verifies it to pave the way for the comprehensive phase noise control in the design-to-manufacture process.

**Methods** To analytically establish the relationship of the coupling coefficient with the aberrations in the form of polynomial expansions, the paper adopts the Fringe Zernike polynomials to represent the aberrations and further construct and describe the wavefront error. Then, the coupling coefficient defined as the modulus of the gradient of the far-field wavefront error is expressed as a polynomial function of the aberration coefficients and the tilt angles and is further simplified on the basis of the symmetry of the telescope. According to this relationship and the aberration characteristics of the telescope design residuals, the paper evaluates the effect of different aberrations on phase noise, revealing that defocus, primary astigmatism, and primary spherical aberration are the keys to controlling the coupling coefficient. Thus, an optimization strategy based on key aberration control is proposed. The performance of this method in far-field phase noise suppression is verified by examples of telescope design.

**Results and Discussions** The wavefront quality of the telescopes before and after optimization (Table 1) by the above strategy is at the  $\lambda/20$  ( $\lambda=1064$  nm) level. Before optimization, the far-field wavefront changes significantly within the range of  $\pm 100$  nrad. Accordingly, the coupling coefficient increases rapidly with the tilt angle to over 1 pm/nrad. After optimization, although the wavefront residuals are slightly worse (Table 2), the range of far-field wavefront error decreases markedly by more than 90% (Fig. 4). The corresponding coupling coefficient is smaller than 0.11 pm/nrad within the range of  $\pm 100$  nrad. It is only 6% of that before optimization and much smaller than the required value (Fig. 5). These results indicate that the optimization strategy based on aberration control can effectively reduce the coupling coefficient of

the far-field phase noise, even in the case of poor wavefront quality.

**Conclusions** On the basis of theoretical analysis of the mechanism of the far-field phase noise, this paper determines the relationship of the coupling coefficient with the aberrations, develops an optimization strategy based on key aberration control, and verifies the strategy. The results reveal that suppressing the key aberrations deliberately instead of simply enhancing the demand for wavefront quality in the optimization process can reduce the sensitivity of the far-field phase to jitters more efficiently, improve the far-field phase stability of the telescope significantly, and balance the severe noise budget and the design freedom of the telescope to reserve sufficient margin for the rest optics.

**Key words** laser optics; telescope; space gravitational-wave detection; far-field phase; coupling coefficient